Aspect-ratio-dependent ultra-low reflection and luminescence of dry-etched Si nanopillars on Si substrate

2009 Nanotechnology 20 035303

(http://iopscience.iop.org/0957-4484/20/3/035303)

Nanotechnology **20** (2009) 035303 (7pp) doi:10.1088/0957-4484/20/3/035303

Aspect-ratio-dependent ultra-low reflection and luminescence of dry-etched Si nanopillars on Si substrate

Yi-Hao Pai[1], Fan-Shuen Meng[1], Chun-Jung Lin[1], Hao-Chung Kuo[2], Shih-Hsin Hsu[3], Yia-Chung Chang[3] and Gong-Ru Lin[1,4]

[1] Graduate Institute of Photonics and Optoelectronics, and Department of Electrical Engineering, National Taiwan University (NTU), 1 Roosevelt Road Section 4, Taipei 106, Taiwan, Republic of China
[2] Department of Photonics and Institute of Electric-Optical Engineering, National Chiao Tung University (NCTU), 1001 Ta Hsueh Road, Hsinchu 300, Taiwan, Republic of China
[3] Research Center for Applied Sciences, Academia Sinica, 128 Academia Road, Sec. 2, Taipei 11529, Taiwan, Republic of China

E-mail: grlin@ntu.edu.tw

Received 8 September 2008, in final form 6 November 2008
Published 16 December 2008
Online at stacks.iop.org/Nano/20/035303

Abstract
The Si nanopillars with high aspect ratio were fabricated by dry-etching the thin SiO_2-covered Si substrate with a rapidly self-assembled Ni nanodot patterned mask. Aspect-ratio-dependent ultra-low reflection and anomalous luminescence of Si nanopillars are analyzed for applications in all-Si based lighting and energy transferring systems. The Si nanopillars induce an ultra-low reflectance and refractive index of 0.88% and 1.12, respectively, at 435 nm due to the air/Si mixed structure and highly roughened surface. The reflectance can be $<10\%$ with a corresponding refractive index of <1.80 between 190 and 670 nm. Lengthening the Si nanopillars from 150 ± 15 to 230 ± 20 nm further results in a decreasing reflectance, corresponding to a reduction in refractive index by $\Delta n/n = 18\%$ in the visible and near-infrared wavelength region. After dry-etching an Si wafer into Si nanopillars, the weak blue-green luminescence with double consecutive peaks at 418–451 nm is attributed to the oxygen defect (O^{2-})-induced radiation, which reveals less relevance with the ultra-low-reflective Si nanopillar surface.

(Some figures in this article are in colour only in the electronic version)

1. Introduction

Over the past few decades, there has been enormous interest in synthesizing semiconductor nanostructures, in which the semiconductor nanorod array has shown its great potential for industrial applications in photonic crystals [1], data storage [2], field electron emitters [3], nanoscale transistors [4, 5] and light-emitting devices [6]. In particular, Si rods, wires or pillars in nanometer scale of low-reflectivity have been comprehensively applied to most optical or photonic components such as semiconductor light-emitting diodes, optical lens system, energy harvesting and transferring optoelectronics, etc. Traditional approaches for fabricating periodic Si nanopillars mainly rely on electron-beam (E-beam) lithography [1, 7–10], which provides accurate size and shape control. Papadimitriou has demonstrated the production of <10 nm Si nanopillar patterned by E-beam lithography [11], however, which is impractical for large-scale fabrication by its low writing speed. Nowadays, noble metal (Au or Ag) based randomized nanodots have emerged as nanomasks to replace the E-beam lithography, and Ni has been considered as an alternative to the noble metals due to its cost-effectiveness and ease of formation features. Not long ago, Yoo *et al* [12] made use of an Ni nanodot mask to

[4] Author to whom any correspondence should be addressed.

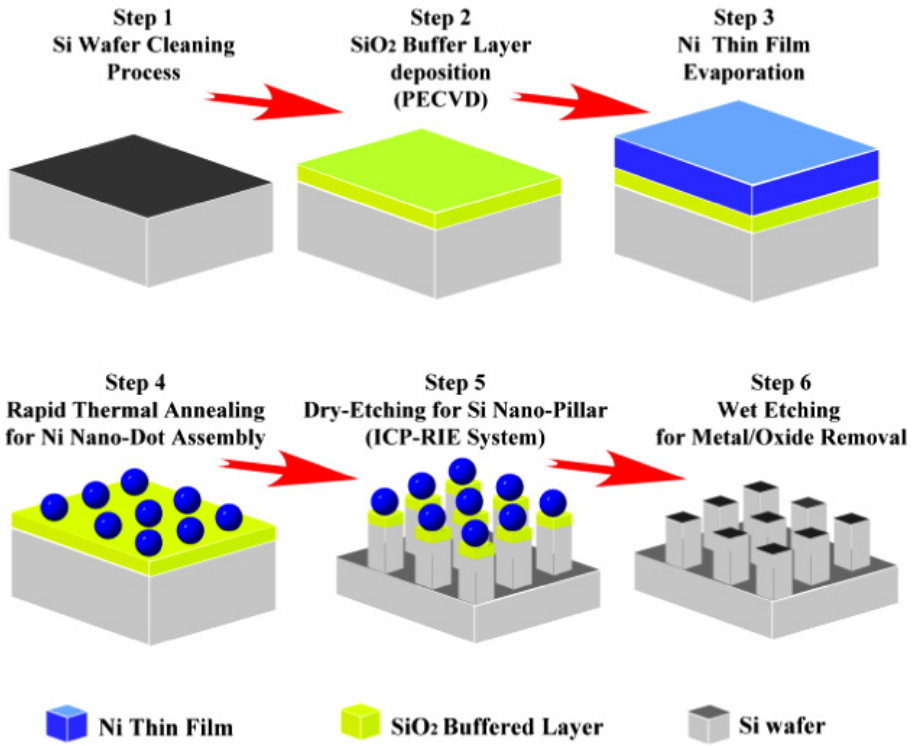

Figure 1. Schematic illustration of Si nanopillars using Ni/SiO_2 as nanomask fabrication.

form high-aspect-ratio Si nanopillars with diameter and height of about 41 nm and 472 nm, respectively. The self-aggregation of an Ni nanodot from Ni film coated on an Si substrate usually takes up to 10 min at 700 °C in N_2 ambient [12]. This is mainly due to the large thermal conductivity of Si substrate, which reduces the thermal energy accumulating on the interface of Ni and Si. Nevertheless, the reported Ni nanodot density is too sparse to enhance the anti-reflection property of the formatted Si nanopillars. The relatively good adhesion at the Ni/Si interface could further slow down the self-aggregation of Ni nanodots [13]. Besides, such a long-term heating process inevitably leads to an unintentional diffusion or alloying of the coated metal into the Si substrate during self-assembly. To avoid the aforementioned problems, we have proposed the quick formation of Ni nanodots on the Si substrate covered with a thin SiO_2, Si_3N_4 [14] or TiN [15, 16] layer. The buffered oxide or nitride layer could prevent the formation of $NiSi_2$ [17] compounds and keep the thermal power concentrated on the Si surface. The Si nanopillars can be formatted by inductively coupled plasma reactive-ion etching (ICP-RIE) of the oxide-covered Si substrate with the mask of self-assembled Ni, Al [18] or Au [19] nanodots. In this work, the optimum ICP-RIE recipes for Si nanopillars with largest aspect ratio are demonstrated. The diameter and density of Si nanopillars or nanorods generated at the Si surface by the ICP-RIE process are characterized. The relationship between ultra-low reflection in the visible and near-infrared (vis–NIR) wavelength range in comparison with other dielectric materials and luminescence of Si nanopillars is investigated and elucidated.

2. Experimental details

The formation procedure of Si nanopillars on Si substrate is illustrated in figure 1, which includes Si wafer cleaning, SiO_2 buffered layer deposition, thin film Ni evaporation, RTA for Ni nanodot assembly, ICP-RIE for Si nanopillars and wet-etching for metal/oxide removal. In more detail, the experimental parameters for optimizing the density of the Ni nanodot mask and improving the aspect ratio of Si nanopillars are listed as below. First of all, the standard cleaning process developed by the company Radio Corporation of America (RCA) is employed to clean the dusty particles and native oxide of a p-type [100] Si wafer. Si wafers are initially immersed in H_2SO_4, NH_4OH, HCl and HF-based solutions to decompose the organic compounds, to get rid of microparticles, to remove alkaline-earth metal and to etch the residual oxide layer, respectively. Afterward, a SiO_2 buffered layer with thickness of 20 nm is deposited by plasma-enhanced chemical vapor deposition (PECVD) with the standard recipe. A 50 nm thick Ni film is evaporated on SiO_2/Si substrate using an E-beam evaporating system with a deposition rate of 0.01 nm s^{-1} at an applied current of 70 mA. Subsequently, the RTA process at 850 °C from 20 to 120 s under N_2 flowing gas of 5 standard cubic centimeter minutes (sccm) is performed to assemble Ni nanodots on the SiO_2/Si substrate. The morphology, dimension and density of Ni nanodots and Si nanopillars are estimated by scanning electron microscopy (SEM, Hitachi FE-SEM S-5000).

The ICP-RIE parameters for different Si nanopillar samples are listed and summarized in table 1. By using an Ni nanodot mask, the Si substrate is dry-etched in a planar

Table 1. The ICP-RIE parameters of Si nanopillar samples are listed and summarized.

Sample number	RF power (W)	DC power (W)	RF/DC ratio (W)	Etching time (min)	Pillar height/diameter (nm/nm)
A	300	100	3	3	$80 \pm 20/65$
B	200	100	2	3	$150 \pm 15/29$
C	100	50	2	5	$250 \pm 20/44$
D	200	200	1	50 (s)	$50 \pm 10/45$

ICP-RIE system (SAMCO ICP-RIE 101iPH) at RF plasma frequency of 13.56 MHz. The RF/DC power ratios set for samples A, B, C and D are 3 (300/100), 2 (200/100), 2 (100/50) and 1 (200/200), respectively. The etching gas of CF_4 and Ar mixture were introduced to substitute the O_2, CF_4, SF_6 and Ar mixture used in earlier experiments. In general, CF_4 is the main gas for etching SiO_2/Si, Ar helps to increase the vertical-etching potential, and O_2 is the mirror gas to accelerate the etching rate. Nevertheless, O_2 is removed from the recipe since it also causes weak oxygen bond and neutral oxygen vacancy defects in Si nanopillars. With the fine-tuning ICP-RIE parameters such as RF/DC power ratio and chamber pressure, Si nanopillars with shrinking diameters below 50 nm can be formatted. The buffered oxide etchant (BOE) was used to remove the Ni-nano-dot/SiO_2 mask layer originally coated over the Si nanopillars prior to our analysis. We characterize the variation on diameter and density of Si nanopillars by comparing different RF and DC power recipes of 100/50 W and 200/100 W with a constant RF/DC power ratio of 2. With corresponding etching time of 3 and 5 min, the optical properties of B and C samples with nearly the same high aspect ratio are compared. The reflectance and refractive index of Si nanopillar samples are measured by using a commercial laser ellipsometer (J A Woollam Co., VASE, 190–900 nm) and confirmed by another ellipsometer (J A Woollam Co., VUV-VASE, 190–1900 nm) covering UV–vis–NIR wavelengths. The luminescence of Si nanopillar samples pumped by an He–Cd laser is characterized using a monochromator in conjunction with a cooled photomultiplier tube (PMT).

3. Results and discussions

To achieve ultra-low reflection, the most popular approach is depositing a multi-dielectric-layer-based anti-reflection coating on the desired samples. Nonetheless, the design on layer thickness and periods is material-independent for such a cost-ineffective technique. Some dielectric films further suffer heating problems due to their low threshold of thermal damage. Alternatively, the surface roughening technique has been applied to versatile solid-state lighting devices for replacing the conventional multi-layer dielectric coating. By taking the Si substrate as an example, the comparison on reflection spectra of the bulk, dielectric-layer-coated, and surface-roughened Si substrates are shown in figure 2. As a result, the reflectance of the bulk Si substrate at <500 nm is dramatically decreased from 45–70% to 30–35% after coating

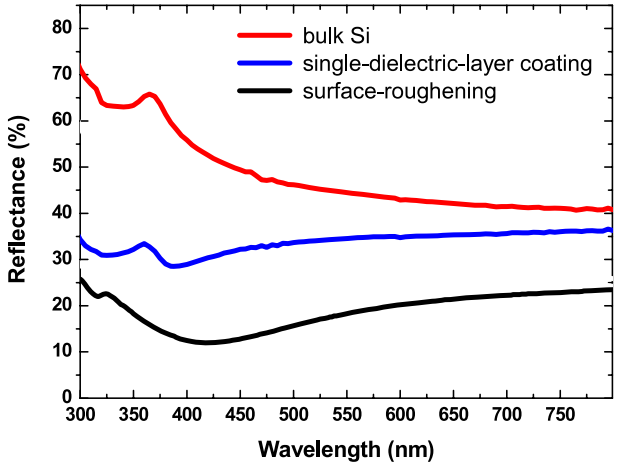

Figure 2. The reflection spectra of bulk, single-dielectric-layer-coated and surface-roughened semiconductor substrate measured at incident angle of 35°.

with a single-layer SiO_2 film. In comparison, the full vis–NIR reflectance of the Si substrate is greatly reduced by a factor of 2–3 after 10 min plasma bombardment under O_2/Ar flowing ratio of 1.25 and RF power of 4.93 W cm^{-2}. The reflectance is below 25% for full spectral range with a minimum of 10% at 400–500 nm. The plasma-induced roughening on the Si surface significantly contributes to a relatively low reflectance as compared to the bulk Si substrate. Surface roughening is indeed a potential candidate for anti-reflection since it effectively releases the concerned issues of damage threshold and adhesion between the dielectric coating and Si substrate. With the aid of nanotechnology, the surface nanoroughness achieved by growing or etching the randomized high-aspect-ratio Si nanopillars has been implemented for the anti-reflection approach. Particularly for Si-based solar cells, both the anti-reflection and hydrophobicity functions are considered to be achieved by roughening the device surface. To meet this demand, it is mandatory to realize how the aspect ratio of Si nanopillars affects the reflection of the Si substrate. The parametric tuning of the dry-etching process for controlling the aspect ratio of Si nanopillars has not yet clearly been understood. In the following sections, the aspect-ratio-dependent reflection and luminescence of Si nanopillars are elucidated in more detail.

3.1. Size and density characterization of rapidly self-assembled Ni nanodot mask

When reviewing the Si nanopillar formation procedure by dry-etching an Si wafer with a metallic nanodot mask, it was found that self-aggregation of the evaporated Ni film on pure Si substrate can hardly be formatted without thermal processing over 10 min. Such a time-consuming step results from the difficulty in self-assembly of Ni nanodots by good adhesion between Ni and Si, which can be solved by depositing a thin SiO_2 layer between Ni and Si. A thin Ni film evaporated on SiO_2 film can easily be conglomerated during the RTA process, leading to a quick formation of Ni nanodots on the

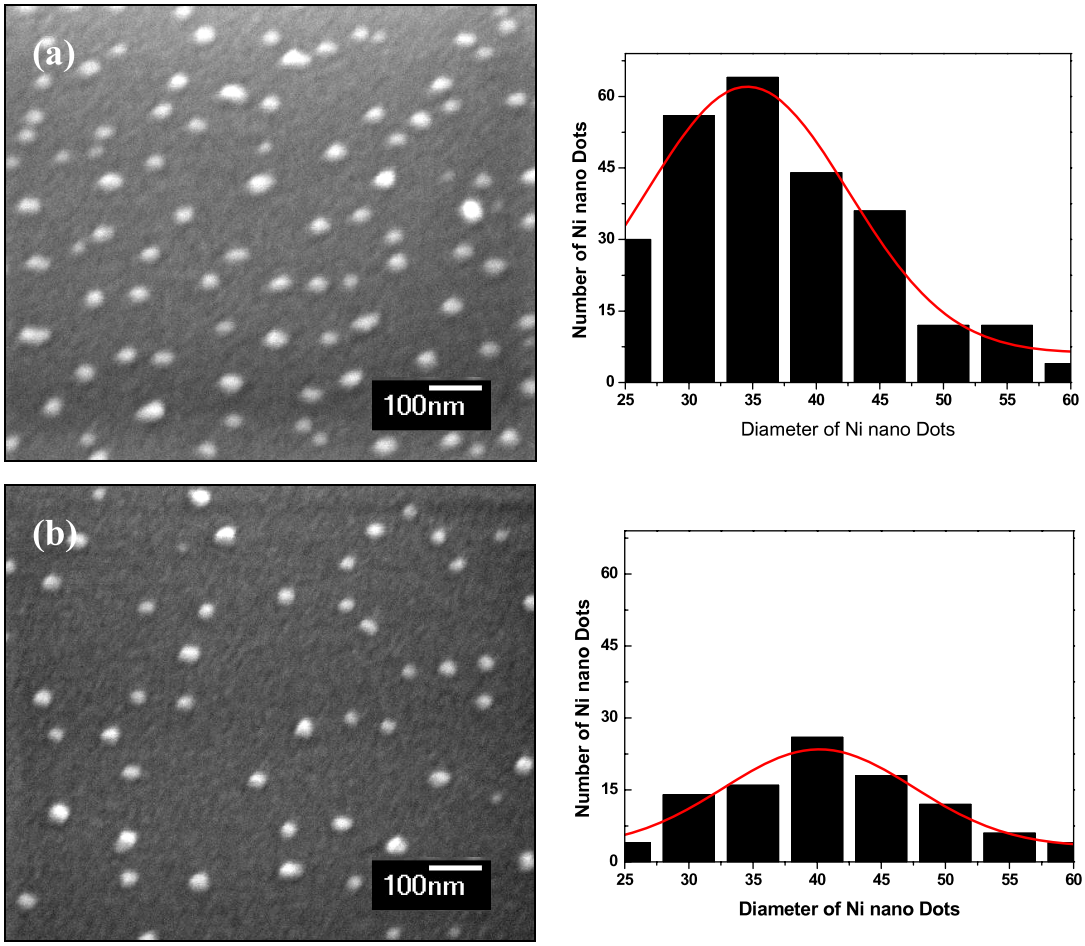

Figure 3. SEM surface morphology of Ni nanodots after different annealing times at 850 °C: (a) 30 s and (b) 120 s.

SiO_2 substrate. Except for decreasing the diameter of Ni nanodots by reducing Ni layer thickness, the thermal energy accumulated at the Ni/SiO_2 interface can be adjusted by annealing temperature and time [13, 14]. Beyond a critical annealing temperature of 850 °C, Ni and Si atoms could obtain sufficient power to form $SiNi_2$ compounds [17]. In contrast, the annealing time needs to be lengthened for congregating Ni nanodots under low temperatures. As shown in figure 3, we compare the effect of the annealing durations on diameter and density of the self-assembled Ni nanodots. The diameter and density of Ni nanodots annealed at 850 °C for 30 s are 37 nm and 1.43 $\times$ 10^{10} cm^{-2}, respectively. By shortening the RTA duration to 22 s, the shape of Ni nanodots becomes hemisphere-like with their average diameter reducing to 33 nm and density increasing to 9.1 $\times$ 10^{10} cm^{-2}.

With increasing RTA time, the Ni atoms obtain more thermal energy to complete their self-aggregation during long-term annealing. In this case, the Ni film only breaks into large strips and eventually self-congregates to larger nanoclusters without approaching a hemispherical shape. For example, the average diameter of Ni nanodots after annealing for 120 s enlarges to 40 nm with decreasing density of 6.7 $\times$ 10^9 cm^{-2}. In more detail, the size distribution of Ni nanodots on an SiO_2 film is mainly determined by SiO_2 film thickness, RTA temperature, RTA time and Ni thickness. The optimized RTA condition for Ni nanodot formation with highest density and smallest diameter is 850 °C for 22 s. The Ni nanodot masked samples prepared under such conditions are selected for subsequent dry-etching of Si nanopillars. In comparison with previous work [12], the density of Ni nanodots (9.1 $\times$ 10^{10} cm^{-2}) is much higher than those previously reported (2.7 $\times$ 10^{10} cm^{-2}). The average diameter of 33 nm for the obtained Ni nanodots is far smaller than the previous record of 60 nm. Moreover, the uniformity of Ni nanodots obtained from our condition is clearly better than in previous works.

3.2. Effect of RF/DC power ratio on density and aspect ratio of Si nanopillars

The ICP-RIE pressure was controlled between 0.66 and 6.66 Pa to detune the etching rate for Si nanopillar formation on Ni nanodot masked SiO_2/Si substrate. The chamber pressure is usually remaining below 0.66 Pa since high-pressure etching fails to form high-aspect-ratio Si nanopillars as the Ni nanodot mask is also etched out concurrently. By changing the RF and DC plasma powers, the shape and aspect ratio of the ICP-RIE Si nanopillars are monitored. Due to the tiny difference between vertical and side etching rates, the isotropic etching further erodes Si nanopillars to approach the smallest density and largest diameter, eventually forming a pyramid shape

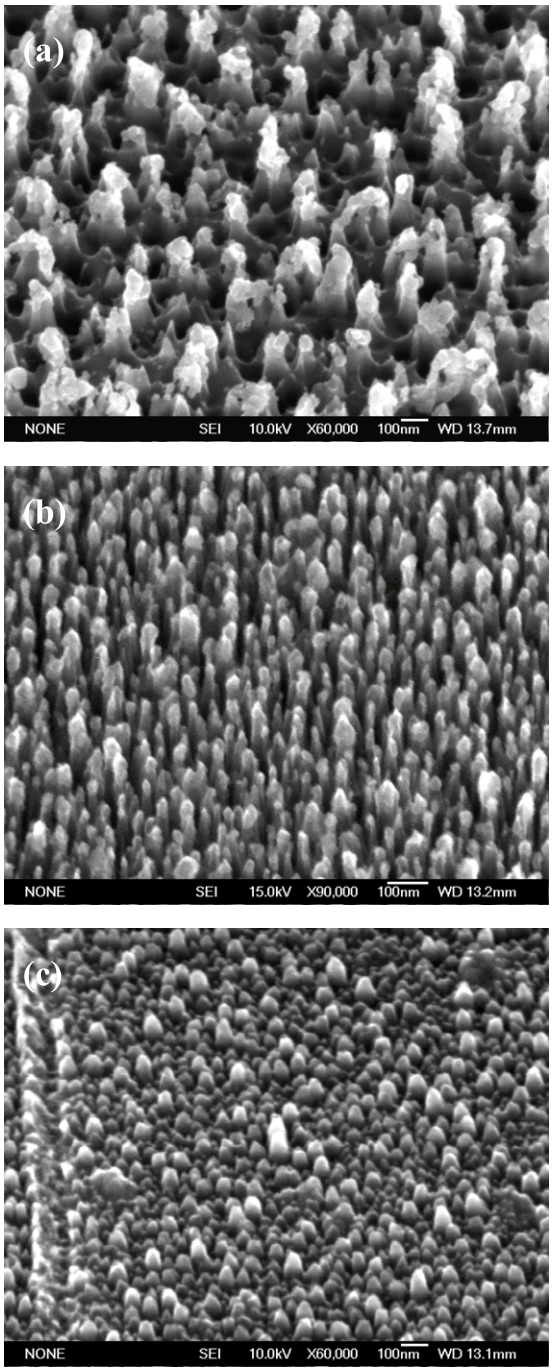

Figure 4. SEM surface morphology of Si nanopillars prepared at (a) RF/DC = 300/100 = 3, (b) RF/DC = 200/100 = 2, and (c) RF/DC = 200/200 = 1.

with large size after long etching duration. In figure 4(a), Si nanopillars with a pyramid-like shape are obtained on sample A under an RF/DC power ratio of 3. Therefore, the RF/DC power ratio is decreased to <3 for obtaining straight Si nanopillars with increasing aspect ratio. As a result, the success in formatting Si nanopillars with a perpendicular sidewall at RF/DC ratio of 2 for sample B is shown in figure 4(b). The density and diameter of Si nanopillars are 3×10^{10} cm^{-2} and 29 nm, respectively. The appropriate RF/DC power ratio is mandatory to form Si nanopillars with

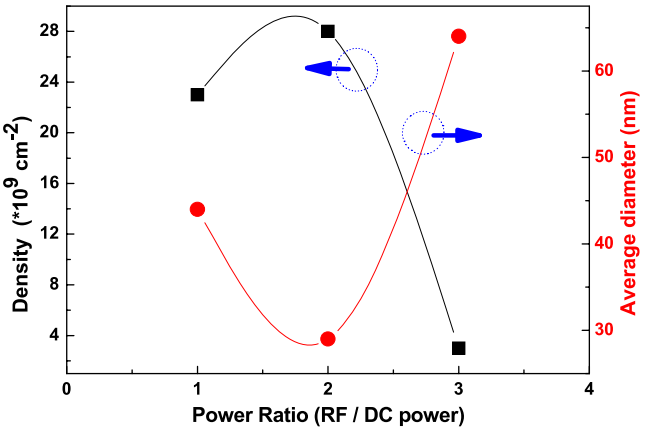

Figure 5. Different ratio of RF/DC has different influence on the vertical level of Si pillar sidewall.

sharp sidewall and large height. In contrast, the straight but short Si nanopillars formatted at an RF/DC power ratio of 1 for sample D is observed, as shown in figure 4(c). In this case, the ICP-RIE fails to balance the selective etching between Ni and Si, leading to the etching of the Ni nanodot mask.

The SEM analysis in figure 5 shows dramatic variation on diameter and density of Si nanopillars formatted under different RF/DC power ratios. Increasing RF/DC power ratio inevitably forms a long but sparse Si nanopillar, whereas the low RF/DC power ratio only leads to dense and short nanopillars. The optimized RF/DC power ratio of 2 is the most suitable condition for etching Si nanopillars with highest aspect ratio. Nonetheless, it is still required to detune the individual RF and DC powers but their ratio remains as constant, which helps to characterize the effect of the etching time on the variation of the height/diameter aspect ratio for Si nanopillars. In comparison with samples C and B with RF/DC powers increased from 100/50 W to 200/100 W at constant RF/DC power ratio, the average Si nanopillar diameter further shrinks from 44 to 29 nm, while the height is also decreased from 230 ± 20 to 150 ± 15 nm. High-plasma-power ICP-RIE is always detrimental to the long Si nanopillar formation. Note that the aforementioned ICP-RIE recipe is oxygen-free to avoid the oxygen-related defects of such O^{2-}, oxygen vacancy, weak oxygen bonds and non-bridged oxygen hole centers occurred in the Si matrix. The maximum aspect ratio of 5.1 obtained for Si nanopillar samples is relatively comparable with that reported by Homma *et al* (up to 7) [19] but less than the value reported by Kim *et al* (up to 12) [12]. Nonetheless, such a high-aspect-ratio dry-etching can be further improved by increasing the etching time at relatively low RF/DC powers. The Si nanopillar diameter can also be reduced to <20 nm by shrinking Ni nanodot size with shortened RTA duration.

3.3. Effect of Si nanopillar aspect ratio on surface reflectance and luminescence

Two kinds of Si nanopillar samples with different etching times (3 and 5 min for sample B and sample C) at the same RF/DC power ratio of 2 were selected to characterize their

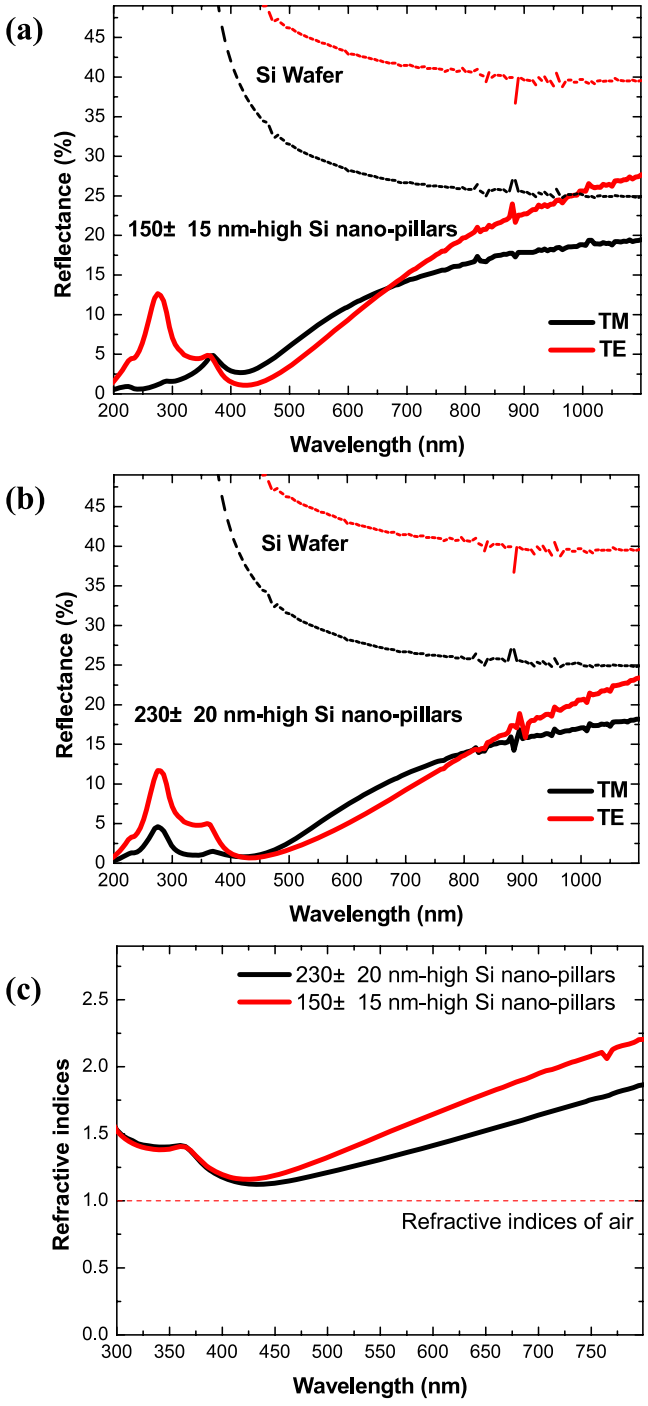

Figure 6. (a), (b) Surface reflectance of Si nanopillars/Si with height of 150 ± 15 nm, 230 ± 20 nm, and Si wafer (inset) measured by using TM and TE polarized beams at incident angle of 35°, (c) the refractive indices of Si nanopillars/Si.

optical reflectance spectra, as shown in figures 6(a) and (b). It is observed that the reflectance of Si nanopillars greatly decreases, but the wavelength-dependent reflectance further exhibits an opposite trend with that of Si wafers between 400 and 1100 nm. The reflectance with a corresponding refractive index of Si nanopillars on Si substrate reaches their minimum of 0.88% and <1.12, respectively, at 400–425 nm. In particular, the effective refractive index of Si

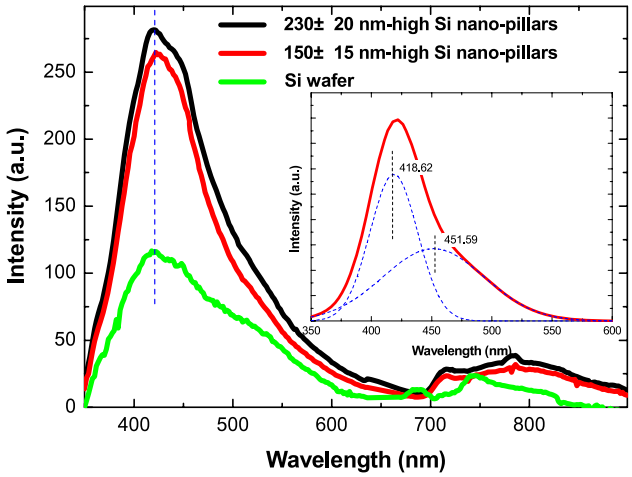

Figure 7. Photoluminescence of Si nanopillars and Si wafer, and peak PL intensities decomposed by two Gaussian fits at 418 and 451 nm at the etching-power ratio of 2 for 3 min (inset).

nanopillars linearly rise with increasing wavelength at 425–900 nm, eventually approaching the refractive index of bulk Si. The index–wavelength slope $\Delta n/\Delta\lambda$ changes from 2.6×10^{-3} to 3×10^{-3} nm^{-1} as Si nanopillar height decreases from 230 ± 20 to 150 ± 15 nm, which is completely different in sign and magnitude from that of bulk Si. Two distinct reflectance peaks at 280 and 370 nm ever observed in bulk Si significantly attenuate after the formation of Si nanopillars with enlarging height. The TE- and TM-mode reflectance spectra of Si nanopillar samples also exhibit extraordinary features from each other at the vis wavelength region. The TE-mode reflectance of Si nanopillar sample is slightly lower than its TM-mode reflectance, which is unusual compared to the nature of the bulk Si at incident angles smaller than the Brewster angle. When increasing Si nanopillar height, such an anomalous phenomenon gradually extends from the vis to NIR wavelength region.

Recently, silica (SiO_2) nanorods with a height of 1.35 μm have been demonstrated to show an ultra-low refractive index of 1.08 [20], using SiO_2 nanorods with both the gap spacing and diameter much smaller than the optical wavelength to minimize Rayleigh and Mie scattering. A similar anti-reflection phenomenon was also found on the micro-porous Si surface, revealing a reduced refractive index of 1.75–2.15 [21]. In our case, the refractive index of 1.12 at 435 nm and <2.0 at wavelengths below 900 nm is obtained for Si nanopillars with average height of 230 ± 20 nm. Another evidence to support the ultra-low refractive index of Si nanopillars is its greatly reduced reflectance at lower incident angles as compared to the unprocessed Si wafer [22]. The reflectance of an Si wafer at an incident angle of 35° is significantly reduced from 36.43% to 0.88% after formatting Si nanopillars, corresponding to a change in refractive index from 4.91 to 1.12. To realize if such an anomalous reflection property of Si nanopillar results from its surface luminescence, the photoluminescence (PL) from Si nanopillars of different aspect ratios are characterized. The results shown in figure 7 indicate that the as-etched Si nanopillars exhibit weak PL at blue-green wavelength due to

the surface-oxidation-induced oxygen defect (O^{2-}) radiation with double consecutive PL peaks. The PL components in our sample prepared at the RF/DC power ratio of 2 for 3 min are very similar to those obtained by Nishikawa *et al* [23] and Bae *et al* [24]. The PL is decomposed by two Gaussian functions at 418 and 451 nm and have been attributed to the transition between the ground state and the elevated state of the NOV defects. In general, Si dangling bounds distributed over such a broad Si nanopillar surface can easily be passivated by oxygen to form a non-stoichiometric thin oxide film. Therefore, the blue PL is enhanced after dry-etching an Si wafer into Si nanopillars, which reveals unchanged central wavelengths and correlated proportionality with the aspect ratio of Si nanopillars.

4. Conclusions

By using the RTA-induced aggregation, a self-assembled Ni nanodot on the thin SiO_2-covered Si substrate as a novel ICP-RIE mask for Si nanopillar formation was successfully demonstrated. The impact of this work is greatly shortening the annealing time to 20 s and increasing the density of Ni nanodots for dense Si nanopillar formation. The maximum density and diameter of Ni nanodots are 9.1×10^{10} cm^{-2} and 37 nm, respectively, formatted under the optimum RTA condition of 850 °C for 22 s. The optimum ICP-RIE recipes for Si nanopillars with highest density and aspect ratio are under a chamber pressure of 0.66 Pa and RF/DC power ratio of 2. After ICP-RIE for 3 min, the obtained density, diameter and height of Si nanopillars are 3×10^{10} cm^{-2}, 29 nm and 150 ± 15 nm, respectively. By increasing the etching time of 5 min, the height of Si nanopillars can be enlarged to 230 ± 15 nm at a reduction of the diameter and density to 44 nm and 1.3×10^{10} cm^{-2}, respectively. The Si nanopillars with a highest aspect ratio of 5.1 causes a reflectance much lower than that of an Si wafer on account of its air/Si mixed structure and highly roughened surface, leading to an ultra-low reflectance and refractive index of 0.88% and 1.12, respectively, at 435 nm. Within the vis to NIR wavelength region (from 190 to 670 nm), the reflectance can be $<10\%$ with a corresponding refractive index of <1.80. In particular, the weak blue PL components are greatly enhanced after dry-etching an Si wafer into Si nanopillars with constant central wavelengths at 418 and 451 nm and correlated proportionality with the aspect ratio of the Si nanopillar due to surface-oxide-dependent radiative states. Nonetheless, the PL intensity only increases slightly with increasing Si nanopillar height, elucidating their irrelevance with the surface ultra-low reflectance. The anomalous ultra-low reflectance of the Si nanopillar has initiated a new research branch of nano-optics, which further motivates the development of Si nanomaterials which benefits from fully processing compatibility with Si-based photovoltaic solar cells.

Acknowledgments

This work was supported in part by the National Science Council (NSC) of the Republic of China, Aim for Top University Project, and Excellent Research Projects of National Taiwan University, Taiwan, ROC, under grants NSC97-2221-E-002-055, 96R0044 and 97R0062-07, respectively.

References

[1] Poborchii V, Tada T and Kanayama T 2002 *Opt. Commun.* **210** 285–90
[2] Sunouchi K *et al* 1989 *IEDM Tech. Dig.* pp 23–6
[3] Karabutov A V, Frolov V D, Smakin A V and Shafeev G A 2001 *IVMC2001: IEEE Proc. 14th Int. Vacuum Microelectronics Conf.* pp 115–6
[4] Terauchi M, Shigyo N, Nitayama A and Horiguchi F 1997 *IEEE Trans. Electron Devices* **44** 2303–5
[5] Bauer F D 2004 *Solid-State Electron.* **48** 705–14
[6] Nassiopoulos A G, Grigoropoulos S and Papadimitriou D 1996 *Appl. Phys. Lett.* **69** 2267–9
[7] Peyrade D, Chen Y, Talneau A, Patrini M, Galli M, Marabelli F, Agio M, Andreani L C, Silberstein E and Lalanne P 2002 *Microelectron. Eng.* **61** 529–36
[8] Francois M, Danlot J, Grimbert B, Mounaix P, Muller M, Vanbesien O and Lippens D 2002 *Microelectron. Eng.* **61** 537–44
[9] Fischer P B, Dai K, Chen E and Chou S Y 1993 *J. Vac. Sci. Technol.* B **11** 2524–7
[10] Liu H I, Biegelsen D K, Johnson N M, Ponce F A and Pease R F W 1993 *J. Vac. Sci. Technol.* B **11** 2532
[11] Nassiopoulos G, Grigoropoulous S, Papadimitriou D and Gogolides E 1995 *Appl. Phys. Lett.* **66** 1114
[12] Kim M J, Lee J S, Kim S K, Yeom G Y, Yoo J B and Park C Y 2005 *Thin Solid Films* **475** 41–4
[13] Zhao J, Sullivan J, Zayac J and Bennett T D 2004 *J. Appl. Phys.* **95** 5475–82
[14] Aballe L, Gregoratti L, Barinov A, Kiskinova M, Clausen T, Gangodadhyay S and Falta J 2004 *Appl. Phys. Lett.* **84** 5031–3
[15] Zhou H and Narayan J 2006 *J. Nanopart. Res.* **8** 595–600
[16] Wang W P, Wen H C, Jian S R, Juang J Y, Lai Y S, Tsai C H, Wu W F, Chen K T and Chou C P 2007 *Appl. Surf. Sci.* **253** 9248–53
[17] Zhou H, Kumar D, Kvit A, Tiwari A and Narayan J 2003 *J. Appl. Phys.* **94** 4841–6
[18] Crouse D, Lo A Y H, Millar E and Crouse M 2000 *Appl. Phys. Lett.* **76** 49–51
[19] Homma Y, Finnie P, Ogino T, Noda H and Urisu T 1999 *J. Appl. Phys.* **86** 3083–8
[20] Xi J Q, Kim J K and Schubert E F 2005 *Nano Lett.* **5** 1385
[21] Chambon E, Florentin E, Torchynska T, Gonzalez-Hernandez J and Vorobiev Y 2005 *Microelectron. J.* **36** 514
[22] Lin G-R, Chang Y C, Liu E S, Kuo H C and Lin H S 2007 *Appl. Phys. Lett.* **90** 181923
[23] Nishikawa H, Stahlbush R E and Stathis J H 1999 *Phys. Rev.* B **60** 15910
[24] Bae H S, Lee W S, Kim T G, Whang C N, Song J H and Im S 2001 *Thin Solid Films* **398/399** 485